Modeling and Design of PCL-Chitosan Bi-Layered Microspheres for Intravitreal Controlled Release

Eduardo A. Chacin Ruiz[a], Samantha L. Carpenter[b,1], Katelyn E. Swindle-Reilly[c,d,e], Ashlee N. Ford Versypt[a,f,g,h,*]

[a]*Department of Chemical and Biological Engineering, University at Buffalo, The State University of New York, Buffalo, NY, USA*
[b]*School of Mechanical and Aerospace Engineering, Oklahoma State University, Stillwater, OK, USA*
[c]*William G. Lowrie Department of Chemical and Biomolecular Engineering, The Ohio State University, Columbus, OH, USA*
[d]*Department of Biomedical Engineering, The Ohio State University, Columbus, OH, USA*
[e]*Department of Ophthalmology and Visual Sciences, The Ohio State University, Columbus, OH, USA*
[f]*Department of Biomedical Engineering, University at Buffalo, The State University of New York, Buffalo, NY, USA*
[g]*Institute for Artificial Intelligence and Data Science, University at Buffalo, The State University of New York, Buffalo, NY, USA*
[h]*Department of Pharmaceutical Sciences, University at Buffalo, The State University of New York, Buffalo, NY, USA*

Abstract

Chronic retinal diseases usually require repetitive dosing. Depending on factors such as dosing frequency, mode of administration, and associated costs, this can result in poor patient compliance. A better alternative involves using controlled release drug delivery systems to reduce the frequency of intravitreal dosing and extend drug release. However, reaching the market stage is a time-consuming process. In this study, we used two computational approaches for estimating the values of the parameters that govern the diffusion-controlled drug release of bovine serum albumin (BSA) and bevacizumab (an agent that slows neovascularization in eye disorders) from bi-layered core-shell microspheres composed of polycaprolactone (PCL) and chitosan. We used the estimated parameters to simulate cumulative release under various conditions to optimize device design to guide future experimental efforts and improve the duration of release above a target daily therapeutic release rate from the microspheres. We explored the impacts of the ratio of polymeric layers and microparticle size on drug release and provided straightforward computational tools for others to reuse for design of bi-layered microspheres.

Keywords: polymeric drug delivery, drug release modeling, mechanistic modeling, sustained drug delivery, polycaprolactone, chitosan

[*]Corresponding author email address: ashleefv@buffalo.edu
[1]Current address: School of Aerospace and Mechanical Engineering, The University of Oklahoma, Norman, OK, USA

1. Introduction

Chronic diseases usually require repeated dosing to maintain therapeutic drug levels over extended periods to manage symptoms and prevent disease progression. Effective controlled-release drug delivery systems (DDSs) offer patient-compliance-enhancing options for treating chronic diseases since they enable sustained drug release for longer periods of time compared with other classic formulations for administration of drugs directly via systemic or localized routes. Different DDS parameters affect the drug release profiles and, therefore, influence the amount and rate of delivery at the target locations. These parameters for layered polymeric DDSs include drug diffusion coefficients, burst release percentage, and drug partition coefficients, which are not necessarily known beforehand. Mathematical modeling of drug release from DDSs can help estimate these parameters, optimize device design, and reduce the amount of experimental work required while improving the treatment of chronic diseases.

Several drug release-controlling mechanisms are discussed in the literature [1–4]: diffusion-controlled, swelling-controlled, and erosion-controlled. Here, we focus on diffusion-controlled release. In the diffusion-controlled mechanism, diffusion through the polymer(s) dominates the drug transport. This mechanism is modeled by Fick's second law, often assuming a constant diffusion coefficient in each material, perfect sink conditions in the medium, and negligible swelling and erosion of the DDS [3, 4]. The analytical solution to the diffusion problem for single-layered DDSs of different ideal geometries (spheres, cylinders, and slabs) is well known [5–10]. However, multi-layered DDSs or DDSs with non-ideal geometries are more complicated and generally need numerical solutions to the governing equations. Several models have been derived from Fick's law with constant diffusivities in each device layer [11–15].

While these previous papers solved the diffusion-controlled drug release problem using fixed values of the drug diffusion coefficient in each different layer (or a drug diffusion coefficient ratio between the layers) and partition coefficient, these values are not always known, and sometimes it becomes necessary to estimate them. There are not many publications on parameter estimation for single-layered [16, 17] or multi-layered spherical devices [18, 19].

For instance, an existing model [18] based on Fick's second law used finite differences in spherical coordinates to estimate the diffusion coefficient of drugs within the core and shell of a capsule. This model considered three domains: core, shell, and bulk (surrounding medium). The model assumed concentration and flux continuity at both interfaces between domains, with a no-mass flux condition imposed at the domain edge. The model was validated using fully 3D lattice Boltzmann simulations, and it was implemented to determine drug diffusion coefficients for both glucose release and absorption scenarios.

Another model [19] was derived to describe drug release from core-shell microparticles. The model considered drug dissolution before drug diffusion and potential drug binding on the shell due to electrostatic interactions. The authors applied the finite elements method in COMSOL. Assumptions included flux and concentration continuity, and perfect sink conditions. The model was used to estimate diffusion coefficients and rate parameters for metronidazole drug release. A sensitivity analysis revealed that the diffusivity in the shell was more sensitive than the diffusivity

on the core.

However, both works considered a unity partition coefficient, did not consider an instantaneous burst release, and have been applied in short-term drug release. This work presents numerical approaches based on finite differences and finite elements for solving the long-term drug release problem and estimating different parameters in diffusion-controlled core-shell spherical DDSs. The numerical methods were applied to estimate the controlling parameters of drug-loaded microspheres composed of polycaprolactone (PCL) and chitosan that attempt to improve wet age-related macular degeneration treatment [20]. The resulting parameters were used to explore the effects of polymer thickness and microparticle size on drug release. The methodology implemented here for bi-layered spherical DDSs can be extended to multi-layered spherical DDSs using the appropriate interface conditions.

2. Methods

2.1. Geometry

The particulate DDS used here is a core-shell microsphere (Figure 1). The radius of the core is R_{core}, and that of the shell is R_{shell}. The shell thickness is denoted $\Delta R = R_{shell} - R_{core}$. We require that $\min \Delta R = 0$, thus $R_{shell} \geq R_{core}$. Note that $\Delta R = 0$ is just the single-layer microsphere case, where $R_{shell} = R_{core}$. Radial symmetry from the center of each microsphere is assumed.

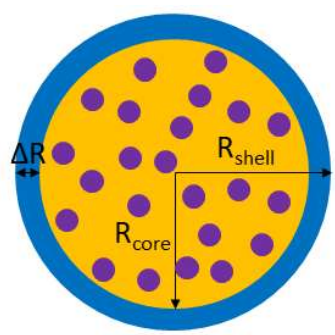

Figure 1: 2D cross-section of a core-shell microsphere. A drug is loaded only in the core. Yellow: core. Blue: shell. Purple: drug. R: radius. $\Delta R = R_{shell} - R_{core}$. Note that the drug is not illustrated to scale.

As test cases, we used data from an experimental study by Jiang et al. [20], where the DDS consisted of a drug-loaded core made of chitosan and a PCL outer shell to protect the chitosan core from degradation and extend drug release. PCL has a very slow hydrolytic degradation rate [21–23]. Bartnikowski et al. [23] combined data from multiple studies in the literature showing that less than 5% of PCL mass was lost by 10 months of *in vitro* degradation in cell-free media at body temperature; Lam et al. [24] showed that the 5% loss threshold was not passed until nearly 2 years. This is much longer than the 6-month time scale in the present study and in Jiang et al. [20]; thus, PCL was assumed to not degrade. Chitosan was shown to degrade by 6 months when

not surrounded by a PCL outer shell but was protected when a shell was present [20]. Thus, we did not consider the case of $\Delta R = 0$ (chitosan single-layered microsphere) as a test case for the diffusion-controlled model. Swelling was also assumed to be negligible for both polymers. Thus, diffusion-controlled release is the dominant release mechanism. In Jiang et al. [20], the mean $R_{core} = 5.10$ μm of chitosan, and the mean $\Delta R = 1.25$ μm of PCL. Two drugs were used Jiang et al. [20] and are considered here: bovine serum albumin (BSA) and bevacizumab, an agent that slows neovascularization in cancer and eye disorders.

2.2. Mathematical model

Fick's second law for time-dependent diffusion is

$$\frac{\partial C}{\partial t} = D\nabla^2 C \tag{1}$$

where $C(\vec{x},t)$ is the drug concentration, $\vec{x}$ refers to the spatial coordinates in either Cartesian or spherical coordinate systems, t is time, and D is a uniform diffusion coefficient. For two concentric layers of a symmetric sphere, this becomes

$$\frac{\partial C}{\partial t} = \begin{cases} \dfrac{D_{core}}{r^2}\dfrac{\partial}{\partial r}\left(r^2\dfrac{\partial C}{\partial r}\right), & 0 \le r \le R_{core} \\[2ex] \dfrac{D_{shell}}{r^2}\dfrac{\partial}{\partial r}\left(r^2\dfrac{\partial C}{\partial r}\right), & R_{core} \le r < R_{shell} \end{cases} \tag{2}$$

where D_{core} and D_{shell} are the diffusion coefficients for the core and shell layers, respectively, and r is the position along the radial dimension.

For the bi-layered or core-shell sphere, there are three boundary conditions to define for $t > 0$ at $r = 0$, R_{core}, and R_{shell}. At the center of the sphere ($r = 0$), the radial symmetry boundary condition is applied:

$$\frac{\partial C(0,t)}{\partial r} = 0 \tag{3}$$

The condition at the interface ($r = R_{core}$) between the two different polymeric domains is the flux continuity condition while allowing for drug partitioning preferentially between the layers based on material properties:

$$D_{core}\frac{\partial C_{core}(R_{core},t)}{\partial r} = D_{shell}\frac{\partial C_{shell}(R_{core},t)}{\partial r} \tag{4}$$

subject to

$$C_{core}(R_{core},t) = \kappa C_{shell}(R_{core},t) \tag{5}$$

where $C_{core}(R_{core},t)$ is the drug concentration in the core at the interface, κ is the partition coefficient, and $C_{shell}(R_{core},t)$ is the drug concentration in the shell at the interface. At the external surface of the sphere ($r = R_{shell}$), the perfect sink condition is assumed: $C(R_{shell},t) = 0$. This

means that all the drug released is immediately cleared away, which is a common assumption in biological tissues.

The initial concentration for the drug-loaded core and non-loaded shell is

$$C(r,0) = \begin{cases} C_{core,0}, & 0 < r \leq R_{core} \\ \\ 0, & R_{core} < r < R_{shell} \end{cases} \tag{6}$$

where $C_{core,0}$ is the initial concentration inside the core, which is set as $C_{core,0} = 1$ arbitrary units (a.u.) for normalizing the concentration calculations.

Drug release is quantified in terms of cumulative release as this metric is often reported in experimental studies. Cumulative release is calculated by

$$Q(t) = B + (100 - B)\left(1 - \frac{\iiint C(\vec{x},t)\,dV}{\iiint C(\vec{x},0)\,dV}\right) \tag{7}$$

where $Q(t)$ is the cumulative percentage of drug released as a function of time, B is the burst release or the percentage of the total drug loaded that is released immediately upon *in vivo* administration or placement into an *in vitro* medium, V is volume, and the last term refers to the fractional amount of drug remaining in the DDS at each time relative to that present in the DDS at initial loading. The total amount of drug in the core-shell microsphere at any time is calculated as the volume-integral of the spatiotemporal distribution of $C(\vec{x},t)$ from the solution of Equations (2)–(6).

The amount of drug released over a time interval $A_{rel}(t)$ is determined using the cumulative release as

$$A_{rel}(t) = \begin{cases} \dfrac{BA_{load,0}}{100}, & \text{if } t = t_0 \\ \\ \dfrac{(Q(t) - Q(t-\Delta t))A_{load,0}}{100}, & \text{if } t > t_0 \end{cases} \tag{8}$$

where t_0 denotes the initial time, Δt is the time interval, and $A_{load,0}$ corresponds to the initial amount of drug loaded into a dose of microspheres. The release rate $R_{rel}(t)$ can be expressed as

$$R_{rel}(t) = \frac{A_{rel}(t)}{\Delta t} \tag{9}$$

which gives the instantaneous average release rate between two time points spaced by Δt. For the particular case of $\Delta t = 1$ day, $R_{rel}(t)$ refers to the drug release rate per day.

2.3. Numerical methods

We solved the model for drug release from the core-shell microsphere DDS defined in Equations (2)–(6) numerically using two alternative approaches: finite differences in MATLAB and finite elements in COMSOl Multiphysics. We compared these two approaches under the same parameter conditions, and the drug concentration results at different locations inside the microspheres were used for verification purposes (Appendix S1 and Figure S1).

2.3.1. Finite differences approach in MATLAB

For the radially symmetric core-shell sphere described in Section 2.1 with uniform diffusion coefficients in each layer and the initial and boundary conditions described in Section 2.2, the finite differences approach is relatively straightforward to implement in technical computing languages such as MATLAB or Python. Here, we used MATLAB. The first step in the approach is to normalize the spherical domain by scaling by R_{shell} so that the domain is $0 < r/R_{shell} < 1$. Then, a variable α is defined as

$$\alpha = \begin{cases} \alpha_{core} = \frac{D_{core}}{R_{shell}^2}, & 0 < \frac{r}{R_{shell}} \leq \frac{R_{core}}{R_{shell}} \\ \alpha_{shell} = \frac{D_{shell}}{R_{shell}^2}, & \frac{R_{core}}{R_{shell}} < \frac{r}{R_{shell}} < 1 \end{cases} \tag{10}$$

to scale the diffusion coefficient by the outer radius and yield a spatially dimensionless form. Note that the time dimension is still included. As defined in Equation (10), α is a piece-wise constant function.

In a technique called the method of lines [25, 26], the partial differential equation (PDE) in Equation (2) with α substituted is transformed into a system of ordinary differential equations (ODEs) by discretizing the normalized spatial domain and using a finite differencing scheme to approximate the spatial derivatives at the discrete points in the domain. The resulting ODEs can be solved using any built-in MATLAB ODE solver; here, we used `ode45`. The classic, second-order-accurate central finite difference discretization scheme in spherical coordinates with uniform grid spacing Δr is [9, 15, 27–29]

$$\frac{dC_m}{dt} = \begin{cases} \frac{6\alpha_0}{\Delta r^2}\left(C_1 - C_0\right), & m = 0; \\ \frac{\alpha_0}{m\Delta r^2}\left((m+1)C_{m+1} - 2mC_m + (m-1)C_{m-1}\right), & m = 1, ..., M-1; \\ 0, & m = M \end{cases} \tag{11}$$

where $C_m(t)$ is the numerical approximation to $C(r_m, t)$ at the grid point $r_m = m\Delta r$ for $m = 0$, 1, ..., M inside the normalized and discretized spherical domain with continuous time t, M is the number of discretizations in the domain, and $\Delta r = 1/M$. Equation (11) holds for a constant value $\alpha_0 = D/R_{shell}^2$ that is uniform throughout a spherical domain. Ford Versypt and Braatz [15] generalized Equation (11) to allow for any function $\alpha(r,t)$, including a piecewise constant function like Equation (10). However, that technique assumed that the grid spacing Δr does not change. A fixed value of Δr could be implemented for select values of R_{core} and R_{shell}; however, here it is desirable to make the algorithm work for arbitrary combinations of R_{core} and R_{shell}. Additionally, the interface boundary condition in Equations (4)–(5) needs to be satisfied. Thus, we adapt Equation (11) as the following schemes in the two layers for solving Equations (2)–(5):

$$\frac{dC_i}{dt} = \begin{cases} \frac{6\alpha_{core}}{\Delta r_{core}^2}\left(C_{i+1} - C_i\right), & i = 0; \\ \frac{\alpha_{core}}{i\Delta r_{core}^2}\left((i+1)C_{i+1} - 2iC_i + (i-1)C_{i-1}\right), & i = 1, ..., I_{core} - 1; \\ \kappa \left.\frac{dC_j}{dt}\right|_{j=0} & i = I_{core}; \end{cases} \tag{12}$$

$$\frac{dC_j}{dt} = \begin{cases} \frac{2\Gamma C_{j+1} - 2(\Gamma+\kappa)C_j + 2C_{i-1}}{\kappa \frac{\Delta r_{core}^2}{\alpha_{core}} + \Gamma \frac{\Delta r_{shell}^2}{\alpha_{shell}}} & j = 0 \text{ and } i = I_{core}; \\ \frac{\alpha_{shell}}{r_j \Delta r_{shell}} \left(C_{j+1} - C_{j-1}\right) + \frac{\alpha_{shell}}{\Delta r_{shell}^2} \left(C_{j+1} - 2C_j + C_{j-1}\right), & j = 1, ..., J_{shell} - 1; \\ 0, & j = J_{shell} \end{cases} \tag{13}$$

where $C_i(t)$ is the numerical approximation to $C(r_i, t)$ at the grid points $r_i = i\Delta r_{core}$ for $i = 0$, 1, $\ldots$, I_{core} inside the core for $0 \leq r/R_{shell} \leq R_{core}/R_{shell}$, $\Delta r_{core} = 1/I_{core}$ is the normalized grid spacing in the core, I_{core} is the number of spatial discretizations in the core, $C_j(t)$ is the numerical approximation to $C(r_j, t)$ at the grid points $r_j = I_{core}\Delta r_{core} + j\Delta r_{shell}$ for $j = 0$, 1, $\ldots$, J_{shell} inside the shell for $R_{core}/R_{shell} \leq r/R_{shell} < R_{shell}/R_{shell}$, $\Delta r_{shell} = 1/J_{shell}$ is the normalized grid spacing in the shell, J_{shell} is the number of spatial discretizations in the shell, and

$$\Gamma = \left(\frac{I_{core}\Delta r_{core} + \Delta r_{core}}{I_{core}\Delta r_{core} - \Delta r_{shell}}\right)\left(\frac{\alpha_{shell}\Delta r_{core}}{\alpha_{core}\Delta r_{shell}}\right) \tag{14}$$

The scheme for the interior points in the shell layer ($j = 1, ..., J_{shell} - 1$) and at the interface ($i = I_{core}$ and $j = 0$) and the relationships between the grid spacing to maintain second-order accuracy are derived in Appendix A.

A total of 300 steps (301 grid points) were used for defining the microsphere domain. We sought to approximate the minimum element size of the COMSOL discretization for the core and then extend more discretization points into the shell portion of the domain. Since the microsphere consists of a chitosan core and a PCL shell, the number of grid points in each layer is proportional to the ratio of the chitosan-to-PCL radius. Drug release was calculated in terms of cumulative release (Equation (7)).

Numerical techniques are used to evaluate the volume integrals with discrete values of $C(\vec{x}, t)$. The MATLAB function `simps` [30] is used to compute the approximate volume integral with discrete values of $C(\vec{x}, t)$ using Simpson's method for numerical integration.

2.3.2. Finite elements approach in COMSOL Multiphysics

COMSOL Multiphysics was used to solve the model equations using the finite elements method. The model geometry is a 2D axisymmetric structure, reducing the 3D problem to a 2D problem by taking advantage of the symmetry about the vertical axis in the 2D plane. The solving procedure involves discretizing the spatial domain into simple geometric elements interconnected to two or more elements at common points. This process results in a system of algebraic equations that must be solved simultaneously. A triangular mesh is used to define the 2D elements in the computational domain. In our implementation, the maximum element size allowed is 0.1 mm, while the minimum element size allowed is 2.4×10^{-5} mm based on the work of Van Kampen et al. [31]. The COMSOL interface "Transport of Diluted Species" is used as the physics package in the software to set up the PDE in Equation (2), to specify the boundary and initial conditions described in Section 2.2, and solve for the time-dependent drug concentration values in the domain. The drug transport equations are set up independently for each layer present in the DDS. At the interface between the layers, a "Partition Condition" boundary condition is used to specify κ.

Numerical techniques are used to evaluate the volume integrals with discrete values of $C(\vec{x},t)$. The COMSOL built-in option `Non-local coupling: integration` was used to evaluate the volume integral with the spatially varying concentration profile of $C(\vec{x},t)$ over the 2D axisymmetric domain that represents a microsphere.

2.4. Sensitivity analysis

We used one-at-a-time sensitivity approaches in MATLAB and COMSOL and the global variance-based Sobol's method [32–34] implemented in COMSOL to assess the sensitivity of the model output to the input parameters. A local sensitivity matrix S is defined with the general form

$$S = \begin{bmatrix} \frac{\partial f(x_1,p)}{\partial p_1} & \dots & \frac{\partial f(x_1,p)}{\partial p_m} \\ \vdots & \ddots & \vdots \\ \frac{\partial f(x_n,p)}{\partial p_1} & \dots & \frac{\partial f(x_n,p)}{\partial p_m} \end{bmatrix} \tag{15}$$

where $f(x_i,p)$ is a model output evaluated at input variable value x_i for $i = 1, \dots, n$ subject to the set of parameters $p = p_1, \dots, p_m$. Generally, the input variables include the independent variable time t, the selected drug, and the geometric properties of the DDS: R_{core} and R_{shell}. Here, we fixed R_{core} and R_{shell} to be the properties of the bi-layered microspheres from Jiang et al. [20] described in Section 2.1. For the model output of interest, we considered the cumulative release at the single time point of 28 days $Q(28)$ from Equation (7) and the model solution of the concentration distribution from Equations (1)–(6) and the set of parameters $p = \{B, D_{core} = D_{Chi}, D_{shell} = D_{PCL}, \kappa\}$. We conducted the analysis for the drugs BSA and bevacizumab.

For the MATLAB local sensitivity analysis, finite differences were used to approximate the derivatives in Equation (15), and each parameter was increased one-at-a-time by 1%. Thus, the normalized local sensitivity $N_{Q(28,p)}$ for the single output for each drug and four parameters is

$$N_{Q(28,p)} = \begin{bmatrix} \frac{Q(28,1.01\times B,D_{Chi},D_{PCL},\kappa)-Q(28,p)}{0.01\times Q(28,p)} \\ \frac{Q(28,B,1.01\times D_{Chi},D_{PCL},\kappa)-Q(28,p)}{0.01\times Q(28,p)} \\ \frac{Q(28,B,D_{Chi},1.01\times D_{PCL},\kappa)-Q(28,p)}{0.01\times Q(28,p)} \\ \frac{Q(28,B,D_{Chi},D_{PCL},1.01\times \kappa)-Q(28,p)}{0.01\times Q(28,p)} \end{bmatrix} \tag{16}$$

In COMSOL, the Morris one-at-a-time (MOAT) method [35–37] and Sobol's method are both available in the uncertainty quantification module [38] and were used while allowing each parameter to be described by a normal distribution and a 1% standard deviation around the baseline value. The cumulative distribution function bounds were defined to constrain the parameter range within $\pm 1\%$ of the baseline value, with the lower bound set at 99% and the upper bound set at 101% of the baseline.

2.5. Parameter estimation

For the estimation of the parameters $p = \{$burst release B, drug diffusion coefficients in the core D_{core} and the shell D_{shell}, and the partition coefficient $\kappa\}$, we used an ordinary least squares objective function with the general form:

$$\min_{p} \sum_{i} [f(xdata_i, p) - ydata_i]^2 \tag{17}$$

where $f(xdata, p)$ is the model output evaluated at values of input variables at which experimental data $ydata$ were collected and i denotes discrete data points. Here, the data are from Jiang et al. [20], and the model outputs of interest are the cumulative release (Equation (7)) values at times $xdata$ when the measurements for experimental cumulative drug release $ydata$ were obtained. As in the sensitivity analysis, R_{core} and R_{shell} were fixed, and the parameter estimation process was conducted for both BSA and bevacizumab.

The MATLAB built-in function `lsqcurvefit` was used for estimating the parameters that minimized the least squares error (Equation (17)). Tolerance was set to 0.001, and the maximum number of objective function evaluations for each parameter update was set to 800. All other optimization settings were at their default values.

We performed a preliminary parameter estimation described in Appendix S2 over in a broad parameter space that yielded feasible cumulative release profiles (see Figure S2 and Table S1). The results from the preliminary parameter estimation allowed us to reduce the parameter space of the problem before refining the parameter estimates. We performed a subsequent parameter estimation using a multi-start process with 50 initial guesses determined by Latin hypercube sampling of the parameter values bounded within the new limits in Table 1. The parameters with the lowest sensitivity were fixed. Upon completing the 50 multi-start parameter estimations, we compared the least squares error values for the parameter sets the `lsqcurvefit` algorithm converged to subject to each of the 50 initial guesses of parameters. The parameter sets from the multi-start parameter estimations that yielded error values within 5% of the minimum error were deemed as acceptable. The resulting parameter values from the acceptable sets were averaged and then simulated for the average model results. Additionally, the parameters from the simulation with the lowest error value were considered the best model parameters. After comparing the best model and the average model, the average parameters were used in all further model simulations.

In COMSOL, we used the built-in `global least-squares objective` function in the optimization module to perform the parameter estimation (Equation (17)) for the four model parameters p. Tolerance was set to 0.001, and maximum function evaluations was set to 1000.

Table 1: Limits used in the multi-start parameter estimation.

Parameter	Lower limit	Upper limit	Units
B	0	20	%
D_{Chi}	1×10^{-15}	1×10^{-13}	cm^2/s

B: burst release. $D_{Chi} = D_{core}$: drug diffusion coefficient in the chitosan core.

2.6. Parameter uncertainty quantification

The sensitivity matrix S from Equation (15) was approximated using the finite differences approach with the MATLAB, and along with the experimental data from cumulative drug release measurements we approximated the variance-covariance matrix [39] by

$$cov(p) = (S^T S)^{-1} S^T \psi S (S^T S)^{-1} \tag{18}$$

where ψ is the covariance of the measurements' matrix. The diagonal elements of this square matrix give the variance of the parameters and can therefore be used to determine the parameters' standard deviation. Finally, using this standard deviation in conjunction with the student's t inverse cumulative distribution function, the 95% confidence interval for the parameters is calculated.

2.7. Code availability

We have provided our codes in a repository at `https://github.com/ashleefv/LayeredSpheres_DDSdesign` [40].

3. Results

3.1. Sensitivity analysis

We observed that the normalized sensitivity of the cumulative drug release at 28 days (Equation (16)) depended on the relative magnitudes of the diffusion coefficients in the chitosan core and the PCL shell (Figure 2). We identified three regimes for these relative magnitudes: $D_{core} << D_{shell}$, $D_{core} \approx D_{shell}$, and $D_{core} >> D_{shell}$. For all the cases shown, the burst and the partition coefficient were tested at the same baseline values of 10 and 1, respectively. Figure 2a, b, and c show the MATLAB local sensitivity results, while Figure 2d, e, and f show the Sobol indices for the global sensitivity results from COMSOL. The sensitivity values from both approaches followed the same patterns regarding the ordering of the sensitivities of the four parameters; however, the insensitive parameters from the Sobol analysis had smaller magnitudes of the sensitivity indices than the corresponding values from the MATLAB local sensitivity analysis. Furthermore, the agreement between first-order and total Sobol indices across all three regimes suggested negligible interaction effects between parameters, indicating that each had an independent influence on cumulative release. These results were consistent with the results from the local MOAT analysis in COMSOL (Appendix S3 and Figure S5).

The most influential parameter depended on the specific regime considered. When drug release was limited by drug diffusion in the chitosan core ($D_{Chi} << D_{PCL}$, Figure 2a,d), the drug diffusion coefficient in the chitosan core D_{Chi} was the most influential parameter with burst release B having a comparable effect. In contrast, the drug diffusion in the PCL shell D_{PCL} and the partition coefficient κ had negligible impacts on the cumulative drug release at 28 days. When the diffusion coefficients were the same ($D_{Chi} = D_{PCL}$, Figure 2b,e), the sensitivity shifted, and the drug diffusion coefficient in the PCL shell D_{PCL} became the dominant parameter, followed by the partition coefficient κ and the drug diffusion coefficient in chitosan D_{Chi}. In this case, burst release B had the lowest impact on

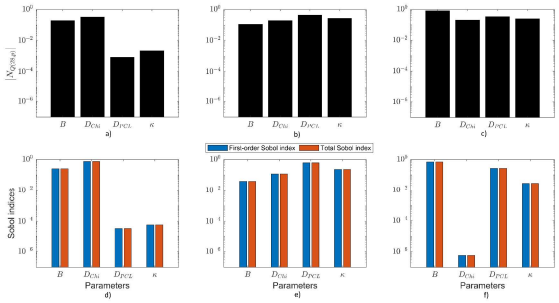

Figure 2: Sensitivity analysis by local and global methods for three regimes of the relative magnitudes of the diffusion coefficients in the chitosan core and the PCL shell. Top row: Absolute value of the normalized sensitivity of the cumulative drug release at 28 days $|N_{Q(28,p)}|$ obtained from the finite differences solution in MATLAB. Each parameter was varied one-at-a-time using a 1% increase. Bottom row: Sobol indices for the sensitivity analysis of parameters affecting cumulative drug release at 28 days obtained using the finite elements solution in COMSOL. For each case, $B = 10$ and $\kappa = 1$. First column: $D_{Chi} << D_{PCL}$. Second column: $D_{Chi} = D_{PCL}$. Third column: $D_{Chi} >> D_{PCL}$. a) and d) $D_{Chi} = 1 \times 10^{-15}$ cm^2/s and $D_{PCL} = 1000 \times D_{Chi} = 1 \times 10^{-12}$ cm^2/s, b) and e) $D_{Chi} = 1 \times 10^{-14}$ cm^2/s and $D_{PCL} = D_{Chi}$, and c) and f) $D_{Chi} = 1 \times 10^{-12}$ cm^2/s and $D_{PCL} = 0.001 \times D_{Chi} = 1 \times 10^{-15}$ cm^2/s. B: burst release. κ: partition coefficient. $D_{Chi} = D_{core}$: drug diffusion coefficient in the chitosan core. $D_{PCL} = D_{shell}$: drug diffusion coefficient in the polycaprolactone shell. Note the difference in y-axis scales between the plots on the two rows.

the cumulative drug release at 28 days. When drug release was limited by drug release in the PCL shell ($D_{Chi} >> D_{PCL}$, Figure 2c,f), the burst release B was the most sensitive parameter, followed by the drug diffusion coefficient in PCL D_{PCL} and partition coefficient κ. In this regime, the drug diffusion coefficient in the chitosan core D_{Chi} had the smallest effect on the cumulative drug release at 28 days.

3.2. Parameter estimation

The preliminary parameter estimation considering all four parameters for both BSA and bevacizumab (Appendix S2) showed that $D_{Chi} << D_{PCL}$ for the chitosan-PCL core-shell microsphere DDS data fitted here (Figures S3 and S4 and Table S2). This parameter regime was insensitive to the parameters D_{PCL} and κ (Figure 2a,d), meaning that their values did not significantly influence the model. Therefore, we set $\kappa = 1$ and $D_{PCL} = 1000 \times D_{Chi}$ and only further refined the parameter estimates for D_{Chi} and B. This reduced model complexity and accelerated the parameter estimation and solution procedure without compromising accuracy.

Figure 3a,b show the error value after each completed parameter estimation for BSA release in MATLAB and COMSOL, respectively. Figure 4a,b are analogous for parameter estimation for bevacizumab release. All of these values were within a 5% error threshold and, therefore, were used when averaging the parameters. Thus, the parameter estimation process was robust to variations in initial guesses for this regime of diffusion coefficients. Figure 3c,d and Figure 4c,d demonstrate that for MATLAB and COMSOL, the average and best (minimum error over all the multi-start parameter estimations) model predictions overlap and are close to experimental data, indicating that the implementation of the model in both software programs can predict BSA and bevacizumab

release from the bi-layered microspheres. Furthermore, Table 2 shows the similarity between the average and best model parameters for each software and the similarity between the best models from both software.

Table 2 also shows the 95% confidence intervals for the uncertainty in parameter values as calculated with the MATLAB results according to Section 2.6. For BSA, burst release had a relatively narrower confidence interval than that for the drug diffusion coefficient in the chitosan core. In contrast, for bevacizumab, the drug diffusion coefficient in the chitosan core had a slightly narrower confidence interval (23% of the parameter's magnitude) and the burst release showed greater variability. For both drugs, the confidence intervals were smaller than the mean values. To facilitate comparison, COMSOL results were rounded to match the number of significant digits from the MATLAB results. Among the parameters estimated in COMSOL, burst release for BSA was the only parameter that fell outside the 95% confidence interval obtained from MATLAB. By visual inspection of Figure 3c,d, the impacts of this minor difference in burst release B values did not impact the results substantially.

Table 2: Estimated parameters for fitting the model to data for drug-loaded chitosan-PCL core-shell microspheres from Jiang et al. [20]. The average model was obtained by averaging the parameters obtained from all the optimization runs that achieved an error within 5% of the minimum error after 100 multi-start attempts. The best model corresponds to the parameter set with the lowest error value.

BSA in MATLAB					
Average model			**Best model**		
Parameter	**Value ± 95% C.I.**	**Units**	**Parameter**	**Value**	**Units**
B	4.6 ± 0.4	%	B	4.72	%
D_{Chi}	$3\times10^{-15} \pm 1\times10^{-15}$	cm^2/s	D_{Chi}	2.88×10^{-15}	cm^2/s
Error value	211.62	-	Error value	209.34	-
BSA in COMSOL					
Average model			**Best model**		
Parameter	**Value**	**Units**	**Parameter**	**Value**	**Units**
B	3.9	%	B	3.86	%
D_{Chi}	3×10^{-15}	cm^2/s	D_{Chi}	2.91×10^{-15}	cm^2/s
Error value	207.20	-	Error value	207.10	-
Bevacizumab in MATLAB					
Average model			**Best model**		
Parameter	**Value ± 95% C.I.**	**Units**	**Parameter**	**Value**	**Units**
B	10 ± 3	%	B	10.3	%
D_{Chi}	$2.6\times10^{-15} \pm 0.6\times10^{-15}$	cm^2/s	D_{Chi}	2.59×10^{-15}	cm^2/s
Error value	435.60	-	Error value	435.06	-
Bevacizumab in COMSOL					
Average model			**Best model**		
Parameter	**Value**	**Units**	**Parameter**	**Value**	**Units**
B	9.6	%	B	9.56	%
D_{Chi}	2.6×10^{-15}	cm^2/s	D_{Chi}	2.59×10^{-15}	cm^2/s
Error value	440.25	-	Error value	440.09	-

B: burst release. $D_{Chi} = D_{core}$: drug diffusion coefficient in the chitosan core. C.I.: confidence interval.

3.3. Predictive capabilities

The computational model was used to explore the impact of both chitosan and PCL layers on cumulative drug release and drug release rate to determine an optimal polymer ratio for beva-

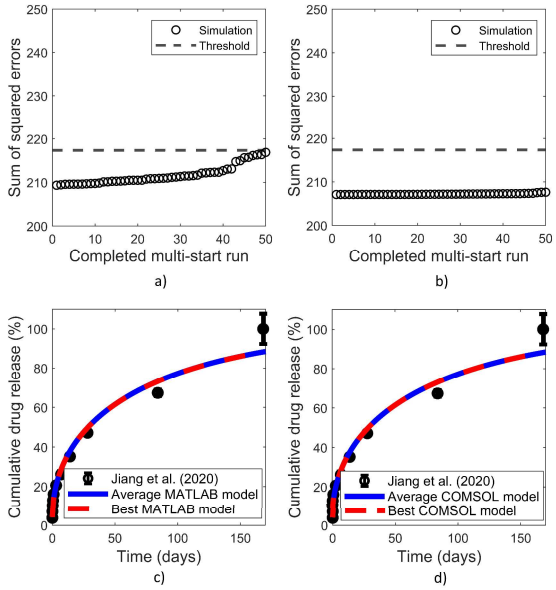

Figure 3: Error value and cumulative drug release profile for BSA release after 50 multi-start parameter estimations. a) Error value in MATLAB. b) Error value in COMSOL. c) Average and best MATLAB models compared to experimental data. d) Average and best COMSOL models compared to experimental data. Experimental data from Jiang et al. [20].

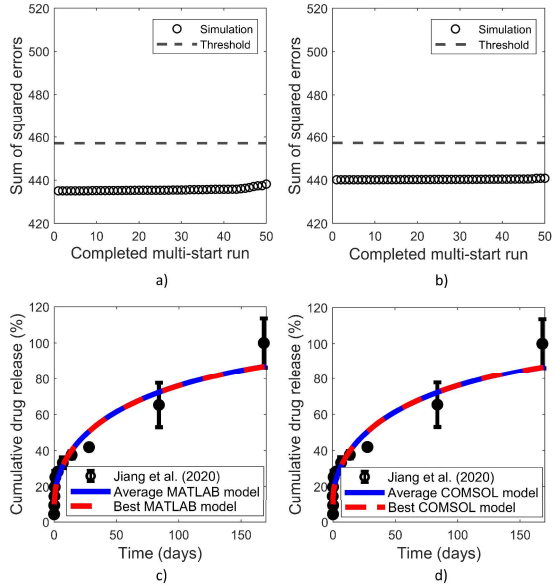

Figure 4: Error value and cumulative drug release profile for bevacizumab release after 50 multi-start parameter estimations. a) Error value in MATLAB. b) Error value in COMSOL. c) Average and best MATLAB models compared to experimental data. d) Average and best COMSOL models compared to experimental data. Experimental data from Jiang et al. [20].

cizumab release using MATLAB. The bevacizumab loaded amount was 1.03 mg [20]. One polymer layer was held constant while the other was varied. The target was to maintain drug release above the estimated threshold as long as possible while ensuring that a substantial portion of the total drug was delivered. The threshold for drug release was derived from a previously published study, which established that an injection of 12.5 µg of bevacizumab was sufficient to reduce neovascularization leakage during a week in patients with proliferative diabetic retinopathy [41]. By dividing the injection amount over 7 days, the approximate threshold can be rounded to 2.0 µg/day. This is consistent with Carichino et al. [42] where it was determined that a retinal anti-VEGF production rate of 1.12–2.62 µg/day would be similarly effective as a ranibizumab injection. The cumulative drug release threshold was set at 90%, since it is representative of practical drug release scenarios and this value is in accordance with Van Kampen et al. [31].

Increasing the radius of the chitosan core (left to right in Figure 5) leads to slower cumulative drug release due to the greater distance through the polymer for the drug to diffuse. A similar but weaker effect is observed when increasing the PCL shell layer (top to bottom in Figure 5). A significant increase in the PCL shell would be required to slow down the cumulative drug release, consistent with the model insensitivity to D_{PCL} in the parameter regime where $D_{core} = D_{Chi}$ controls the release. For the fastest cumulative drug release (top left in Figure 5), the 90% cumulative release threshold is achieved between 12–13 days, whereas for the slowest cumulative drug release (bottom right) only about 70% of the loaded drug is released by 6 months. Figure 6 shows the increase in time to reach the 90% cumulative release as R_{core} and ΔR increase.

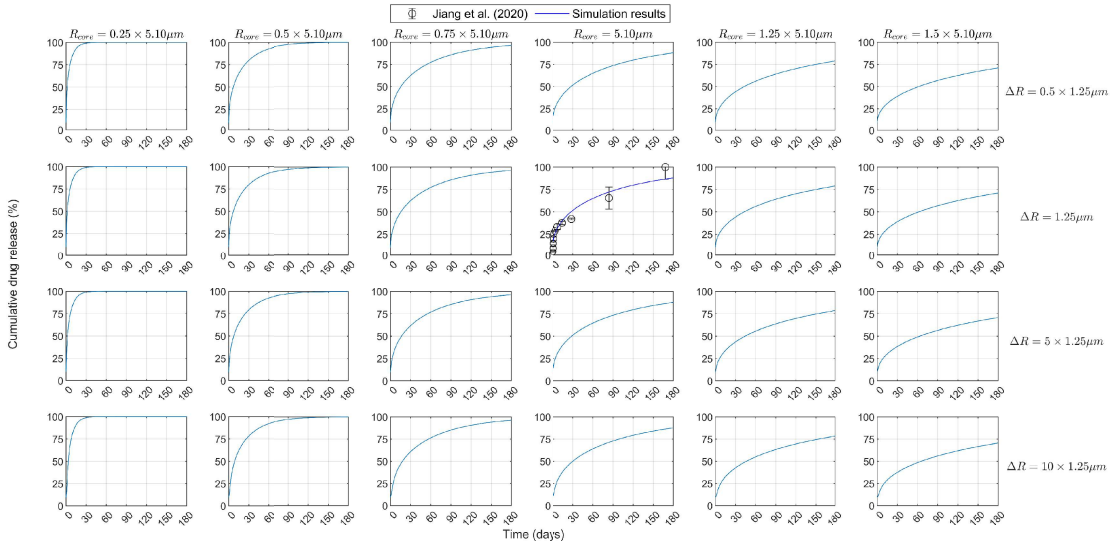

Figure 5: Cumulative bevacizumab release for the different chitosan-PCL configurations. $\Delta R = R_{shell} - R_{core}$ and mention the materials used for the two layers. Experimental data from Jiang et al. [20].

Figure 7 shows that reducing the chitosan core radius below the baseline results in a faster release, shortening the duration of a therapeutic delivery. In contrast, increasing the chitosan radius

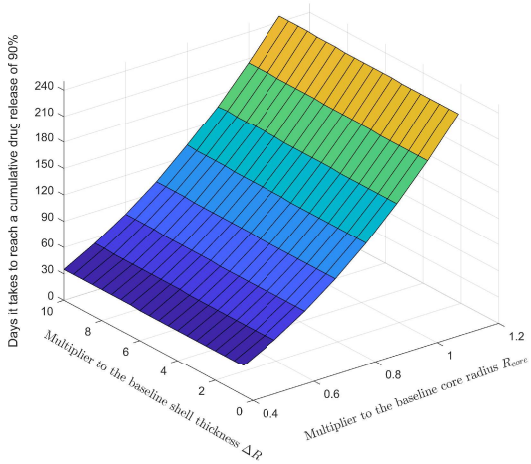

Figure 6: Cumulative bevacizumab release surface plot for the different chitosan-PCL configurations. Cumulative drug release threshold set at 90%. $\Delta R = R_{shell} - R_{core}$ and mention the materials used for the two layers.

of up to 1.5 times its baseline value is not significantly beneficial for the drug release rate. Furthermore, variations on the PCL layer have little effect on the drug release rate, and a substantial increase in the PCL layer would be needed to observe any significant change in the release rate. For instance, for baseline chitosan and PCL, a 10-fold increase on the PCL layer only extends the 2 μg/d drug release rate from 111 days to 114 days. Additionally, considering a $\pm 10\%$ the release rate threshold gives a range of days in which a therapeutic release could be reached. The size of this therapeutic range increases with the chitosan radius. Figure 8 shows that a maximum time above the 2 μg/d threshold is reached around the baseline chitosan value and that PCL has little effect.

Figure 9a illustrates the intersection of surface plots for threshold cumulative drug release and drug release rate. The ideal microparticle configuration is one that sustains a bevacizumab release of 2 μg/day release while maximizing drug depletion (90% cumulative release). As shown in Figure 9b,c a microparticle with around $0.65 \times R_{core}$ and $1\text{–}10 \times \Delta R$ can maintain a therapeutic release rate and achieve 90% drug depletion within 90 days.

4. Discussion

The relative importance of the parameters in the sensitivity analysis depended on the specific regime considered. In the regime where $D_{core} >> D_{shell}$, our sensitivity analysis results are consistent with the findings from Barchiesi et al. [19]. The authors showed that when $D_{core}/D_{shell} \approx 10$, the diffusivity in the shell was significantly more influential than the diffusivity in the core.

The difference between drug diffusion coefficients in the PCL shell between MATLAB and COMSOL are likely related to the lack of sensitivity of this parameter in the model, since it has a limited impact on the overall drug release profile.

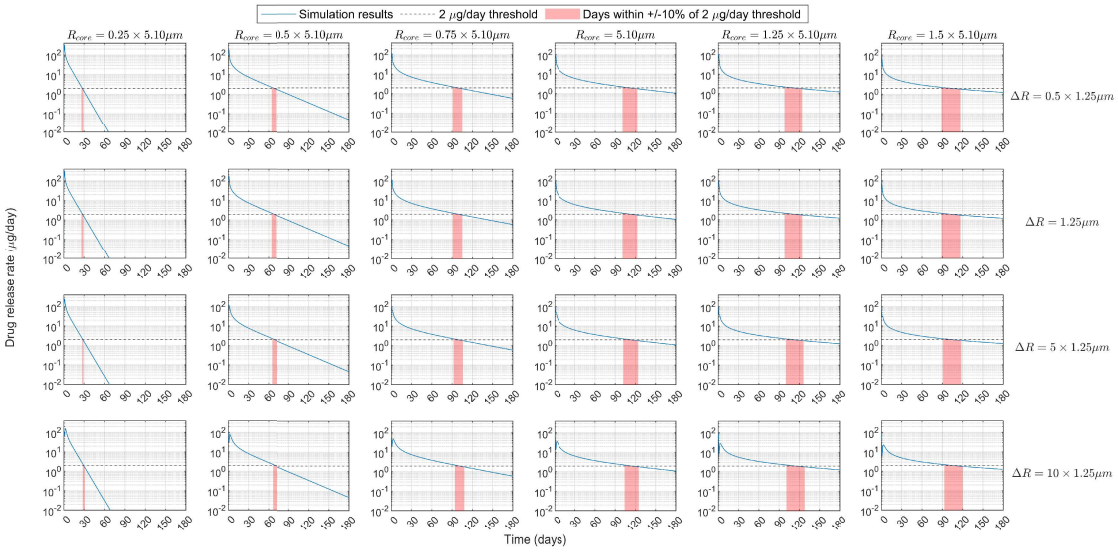

Figure 7: Bevacizumab release rate for the different chitosan-PCL configurations. $\Delta R = R_{shell} - R_{core}$ and mention the materials used for the two layers.

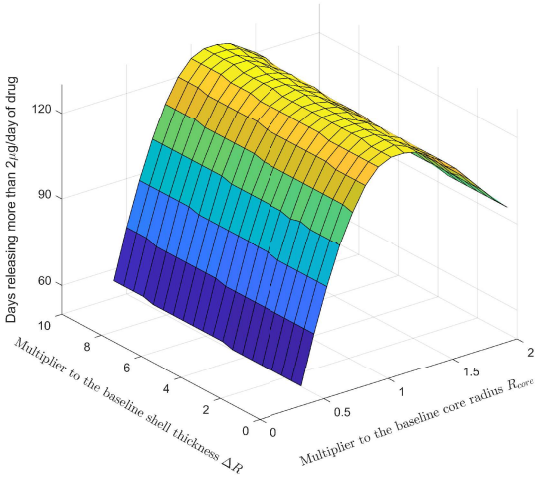

Figure 8: Bevacizumab release rate surface plot for the different chitosan-PCL configurations. Drug release rate threshold was set at 2 µg/day. $\Delta R = R_{shell} - R_{core}$ and mention the materials used for the two layers.

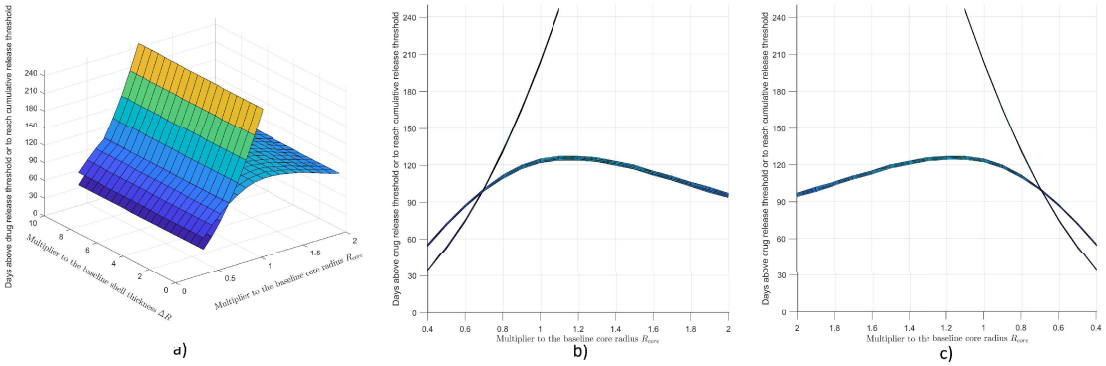

Figure 9: Combined bevacizumab cumulative release and release rate surface plots for the different chitosan-PCL configurations. a) 3D view of the intersection between both surfaces. b) 2D view of the intersection between both surfaces from the perspective of ΔR = 0.5. c) 2D view of the intersection between both surfaces from the perspective of ΔR = 10. Cumulative drug release threshold set at 90%. Drug release rate threshold was set at 2 µg/day. $\Delta R = R_{shell} - R_{core}$ and mention the materials used for the two layers.

Since the standard deviations of the parameters are smaller than the mean values, that means that the parameters are practically identifiable given that the parameters sign is consistent. For BSA, burst release appears to be more predictable as suggested by its lower standard deviation. In contrast, for bevacizumab, the tight confidence interval in drug diffusion in the core suggest that this parameter governs the drug release. The differences in variability could be attributed to the size difference between BSA and bevacizumab, which likely influences how dominant each parameter is for drug release.

The 50 multi-start parameter estimations in MATLAB required 12–16 days to complete using parallel computing on a machine with eight cores. The multi-start parameter estimations in COMSOL took around 6 days, and each subsequent estimation involved manually changing the initial guesses. The MATLAB model was used to explore different design parameters in the chitosan-PCL core-shell microsphere DDS, since it offers a slightly faster forward problem-solving compared to COMSOL and offers greater ease of automation. While both software provided similar results, COMSOL's capability for handling more complex geometries can be advantageous on cases where simple approximations are not sufficient.

While increasing R_{core} or ΔR slows cumulative drug diffusion, an increase in R_{core} from its baseline value has little effect on drug release rate until it exceeds $1.5\times R_{core}$ where the release rate begins to decline. Conversely, reducing R_{core} accelerates drug release, shortening the duration above the release rate threshold. ΔR increase needs to be significant to observe a small increase on the days the drug release rate stays above the threshold. This implies that tuning R_{core} is the best way to optimize the therapeutic delivery and that ΔR adjustments need to be significant for meaningful drug release modifications.

The best configuration for sustained therapeutic release and efficient drug depletion is around the $0.65\times R_{core}$ and $1\text{–}10\times\Delta R$ since this design releases more than 2 µg/day of bevacizumab for 90

days while achieving a 90% cumulative drug release.

5. Conclusions

The models were verified by comparing the drug concentration profiles at different locations within the microspheres. The results showed good agreement between both models. However, new data is still required for the validation of our models.

Both finite differences (MATLAB) and finite elements (COMSOL) approaches were able to predict drug release behavior from the BSA- and bevacizumab-loaded microspheres. The average parameter values for both approaches tend to be close. We only performed 50 simulations due to the computational cost, but it is expected that the higher the number of simulations, the closer these average models should be. Furthermore, the models tend to be more effective (lower error values) the lower the standard deviations on the experimental data are.

Determining parameters like drug diffusion coefficient in the polymers, burst release, and drug partition coefficient helps to better understand drug release from the bi-layered microspheres. This information can be used to optimize device design computationally to guide experiments and improve chronic disease treatments, as it was shown that a reduction in the chitosan layer or the total microparticle size is beneficial for therapeutic drug release. The methods described here can be applied to any diffusion-controlled bi-layered microsphere. They can even be extended to multiple layers to attempt to improve therapies that require long-term release.

Appendix A. Derivation of finite difference schemes

Appendix A.1. Interior nodes

The finite difference equations for diffusion in a sphere with the initial and outer boundary conditions defined in Section 2.2 are well-known and are shown in Equations (12) and (13) for $i = 0$ and $j = J_{shell}$. The finite difference scheme for the interior nodes of the core layer are also in a standard form for $i = 1, ..., I_{core} - 1$ in Equation (12). Here, we first rewrite that interior form to consider how the radial position impacts the scheme to generalize to the case that the grid spacing is not uniform and the indexing restarts in the shell layer. Let $\hat{r}$ be the radial position from the center of the sphere and r be the normalized radial position, where $r = \hat{r}/R_{shell}$. The diffusion equation in dimensionless spherical coordinates using α from Equation (10) and expanding the derivative in Equation (2) gives

$$\frac{\partial C}{\partial t} = \begin{cases} \dfrac{2\alpha_{core}}{r}\dfrac{\partial C}{\partial r} + \alpha_{core}\dfrac{\partial^2 C}{\partial r^2}, & 0 < r < R_{core}/R_{shell} \\ \\ \dfrac{2\alpha_{shell}}{r}\dfrac{\partial C}{\partial r} + \alpha_{shell}\dfrac{\partial^2 C}{\partial r^2}, & R_{core}/R_{shell} < r < 1 \end{cases} \tag{A1}$$

Applying centered finite differences for $0 < r < R_{core}/R_{shell}$ gives

$$\frac{dC_i}{dt} = \frac{\alpha_{core}}{r_i \Delta r_{core}}\left(C_{i+1} - C_{i-1}\right) + \frac{\alpha_{core}}{\Delta r_{core}^2}\left(C_{i+1} - 2C_i + C_{i-1}\right), \quad i = 1, ..., I_{core} - 1; \tag{A2}$$

which can be rewritten as

$$\frac{dC_i}{dt} = \frac{\alpha_{core}}{\Delta r_{core}^2}\left(\frac{r_{i+1}}{r_i}C_{i+1} - 2\frac{r_i}{r_i}C_i + \frac{r_{i-1}}{r_i}C_{i-1}\right), \quad i = 1, ..., I_{core} - 1; \tag{A3}$$

In the core, $r_i = i\Delta r_{core}$, $r_{i+1} = (i+1)\Delta r_{core}$, and $r_{i-1} = (i-1)\Delta r_{core}$, yielding the familiar form:

$$\frac{dC_i}{dt} = \frac{\alpha_{core}}{i\Delta r_{core}^2}\left((i+1)C_{i+1} - 2iC_i + (i-1)C_{i-1}\right), \quad i = 1, ..., I_{core} - 1; \tag{A4}$$

Repeating the derivation of Equation (A3) for $R_{core}/R_{shell} < r < 1$ gives

$$\frac{dC_j}{dt} = \frac{\alpha_{shell}}{r_j\Delta r_{shell}}\left(C_{j+1} - C_{j-1}\right) + \frac{\alpha_{shell}}{\Delta r_{shell}^2}\left(C_{j+1} - 2C_j + C_{j-1}\right), \quad j = 1, ..., J_{shell} - 1; \tag{A5}$$

and

$$\frac{dC_j}{dt} = \frac{\alpha_{shell}}{\Delta r_{shell}^2}\left(\frac{r_{j+1}}{r_j}C_{j+1} - 2\frac{r_j}{r_j}C_j + \frac{r_{j-1}}{r_j}C_{j-1}\right), \quad j = 1, ..., J_{shell} - 1; \tag{A6}$$

Unlike in the core, the coordinates in the shell are $r_j = R_{core}/R_{shell} + j\Delta r_{shell}$, $r_{j+1} = R_{core}/R_{shell} + (j+1)\Delta r_{shell}$, and $r_{j-1} = R_{core}/R_{shell} + (j-1)\Delta r_{shell}$. Thus, Equation (A5) is adopted for the interior points in the shell layer with $r_j = I_{core}\Delta r_{core} + j\Delta r_{shell}$. The compact forms in Equations (A3) and (A6) are used in the derivation of the interface equations.

Appendix A.2. Interface

As the interface condition defined in Equations (4) and (5) allows for two different values at the interface, we need to devise schemes for calculating both of these values. We adopt the fictitious node method [9, 43], which was used for the derivation of the scheme for the boundary condition at the center of the sphere. Figure A1 illustrates the discrete points near the interface, with an additional grid point at r_{i+1} that is considered to extend the core past the interface by Δr_{core} into the shell and another at r_{j-1} that extends the shell beyond the interface by $-\Delta_{shell}$ into the core. Then, the interior point schemes from Equations (A3) and (A6) can be used. However, the values of the fictitious points need to be determined. We use the interface condition to determine equations for these points.

We apply the normalized radial position and insert α from Equation (10) to yield

$$\alpha_{core}\frac{\partial C_{core}(R_{core}/R_{shell}, t)}{\partial r} = \alpha_{shell}\frac{\partial C_{shell}(R_{core}/R_{shell}, t)}{\partial r} = F \tag{A7}$$

where F is the continuous flux at the interface $r = R_{core}/R_{shell}$. Using the centered difference approximation around $i = I_{core}$ and $j = 0$ at the interface (Figure A1) gives

$$\alpha_{core}\left(\frac{C_{i+1} - C_{i-1}}{2\,\Delta r_{core}}\right) = \alpha_{shell}\left(\frac{C_{j+1} - C_{j-1}}{2\Delta r_{shell}}\right) = F \tag{A8}$$

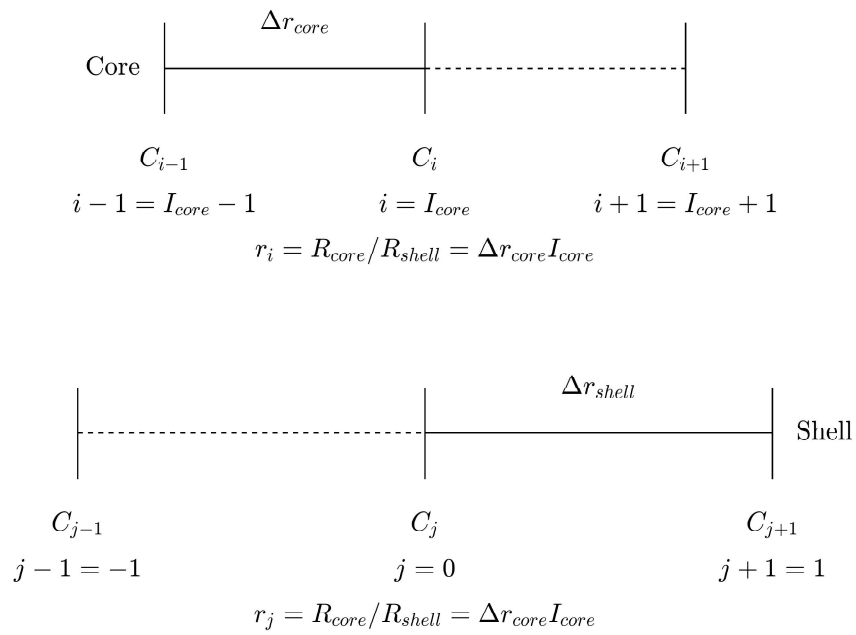

Figure A1: Fictitious node method applied to the interface between two layers of a sphere. C_i and C_j denote the concentrations at the interface in the core and shell layers, respectively. The fictitious points are C_{i+1} and C_{j-1}. Δr_{core} and Δr_{shell} are not shown to scale; the key point is that they do not need to be equal.

Equation (A8) can be rearranged to solve for the fictitious points C_{i+1} and C_{j-1} as functions of F:

$$C_{i+1} = C_{i-1} + \frac{2F\Delta r_{core}}{\alpha_{core}} \tag{A9}$$

$$C_{j-1} = C_{j+1} - \frac{2F\Delta r_{shell}}{\alpha_{shell}} \tag{A10}$$

Inserting Equations (A9) and (A10) into Equations (A3) and (A6) at the interface ($i = I_{core}$ and $j = 0$) gives

$$\frac{dC_i}{dt} = \frac{\alpha_{core}}{\Delta r_{core}^2}\left(\frac{r_{i+1}}{r_i}\left(C_{i-1} + \frac{2F\Delta r_{core}}{\alpha_{core}}\right) - 2\frac{r_i}{r_i}C_i + \frac{r_{i-1}}{r_i}C_{i-1}\right) \tag{A11}$$

and

$$\frac{dC_j}{dt} = \frac{\alpha_{shell}}{\Delta r_{shell}^2}\left(\frac{r_{j+1}}{r_j}C_{j+1} - 2\frac{r_j}{r_j}C_j + \frac{r_{j-1}}{r_j}\left(C_{j+1} - \frac{2F\Delta r_{shell}}{\alpha_{shell}}\right)\right) \tag{A12}$$

These equations simplify to

$$\frac{dC_i}{dt} = \frac{\alpha_{core}}{\Delta r_{core}^2}\left(2\left(C_{i-1} - C_i\right) + \frac{r_{i+1}}{r_i}\left(\frac{2F\Delta r_{core}}{\alpha_{core}}\right)\right) \tag{A13}$$

and

$$\frac{dC_j}{dt} = \frac{\alpha_{shell}}{\Delta r_{shell}^2}\left(2\left(C_{j+1}-C_j\right) - \frac{r_{j-1}}{r_j}\left(\frac{2F\Delta r_{shell}}{\alpha_{shell}}\right)\right) \tag{A14}$$

Rearranging to solve for F in both equations and equating them gives

$$F = \frac{r_i\alpha_{core}}{2r_{i+1}\Delta r_{core}}\left(\frac{dC_i}{dt}\frac{\Delta r_{core}^2}{\alpha_{core}} - 2\left(C_{i-1}-C_i\right)\right) = \frac{r_j\alpha_{shell}}{2r_{j-1}\Delta r_{shell}}\left(2\left(C_{j+1}-C_j\right) - \frac{dC_j}{dt}\frac{\Delta r_{shell}^2}{\alpha_{shell}}\right) \tag{A15}$$

Now that F has been eliminated, the partition coefficient from Equation (5) can be applied, i.e., $C_i = \kappa C_j$ at the interface. Also, applying derivatives with respect to time at the interface, we have that

$$\frac{dC_i}{dt} = \kappa\frac{dC_j}{dt}\bigg|_{j=0} \quad i = I_{core} \tag{A16}$$

Thus, Equation (A15) yields

$$\frac{r_i\alpha_{core}}{2r_{i+1}\Delta r_{core}}\left(\kappa\frac{dC_j}{dt}\frac{\Delta r_{core}^2}{\alpha_{core}} - 2\left(C_{i-1}-\kappa C_j\right)\right) = \frac{r_j\alpha_{shell}}{2r_{j-1}\Delta r_{shell}}\left(2\left(C_{j+1}-C_j\right) - \frac{dC_j}{dt}\frac{\Delta r_{shell}^2}{\alpha_{shell}}\right) \tag{A17}$$

Inserting

$$\gamma = \frac{\alpha_{shell}\,\Delta r_{core}}{\alpha_{core}\,\Delta r_{shell}} \tag{A18}$$

and moving all the r values to the right-hand side gives

$$\kappa\frac{dC_j}{dt}\frac{\Delta r_{core}^2}{\alpha_{core}} - 2\left(C_{i-1}-\kappa C_j\right) = \gamma\frac{r_j r_{i+1}}{r_{j-1}r_i}\left(2\left(C_{j+1}-C_j\right) - \frac{dC_j}{dt}\frac{\Delta r_{shell}^2}{\alpha_{shell}}\right) \tag{A19}$$

Letting

$$\Gamma = \gamma\frac{r_{i+1}}{r_{j-1}}, \tag{A20}$$

remembering that $r_i = r_j$ at the interface, and rearranging to group like terms

$$\frac{dC_j}{dt}\left(\kappa\frac{\Delta r_{core}^2}{\alpha_{core}} + \Gamma\frac{\Delta r_{shell}^2}{\alpha_{shell}}\right) = 2\Gamma C_{j+1} - 2\left(\Gamma+\kappa\right)C_j + 2C_{i-1} \tag{A21}$$

Solving for the derivative at the interface yields

$$\frac{dC_j}{dt} = \frac{2\Gamma C_{j+1} - 2\left(\Gamma+\kappa\right)C_j + 2C_{i-1}}{\kappa\frac{\Delta r_{core}^2}{\alpha_{core}} + \Gamma\frac{\Delta r_{shell}^2}{\alpha_{shell}}} \quad j = 0 \text{ and } i = I_{core} \tag{A22}$$

Acknowledgments

This work was supported by National Institutes of Health grant R35GM133763 to ANFV, R01EB032870 to KESR and ANFV, Owen Locke Foundation to KESR, and the University at Buffalo. We thank lab members for their thorough feedback on this manuscript and helpful discussions.

References

[1] Chacin Ruiz, E.A.; Swindle-Reilly, K.E.; Ford Versypt, A.N. Experimental and mathematical approaches for drug delivery for the treatment of wet age-related macular degeneration. *J. Controlled Release* **2023**, *363*, 464–483.

[2] Ford Versypt, A.N.; Pack, D.W.; Braatz, R.D. Mathematical modeling of drug delivery from autocatalytically degradable PLGA microspheres–a review. *J. Controlled Release* **2013**, *165*, 29–37.

[3] Kanjickal, D.G.; Lopina, S.T. Modeling of drug release from polymeric delivery systems–a review. *Crit. Rev. Ther. Drug Carrier Syst.* **2004**, *21*, 345–386.

[4] Siepmann, J.; Siepmann, F. Mathematical modeling of drug delivery. *Int. J. Pharm.* **2008**, *364*, 328–343.

[5] Baker, R. *Controlled Release of Biologically Active Agents*; John Wiley & Sons: New York, NY, USA, 1987.

[6] Higuchi, T. Rate of release of medicaments from ointment bases containing drugs in suspensions. *J. Pharm. Sci.* **1961**, *50*, 874—875.

[7] Roseman, T.J.; Higuchi, W.I. Release of medroxyprogesterone acetate from a silicone polymer. *J. Pharm. Sci.* **1970**, *59*, 353–357.

[8] Roseman, T.J. Release of steroids from a silicone polymer. *J. Pharm. Sci.* **1972**, *61*, 46–50.

[9] Crank, J. *The Mathematics of Diffusion*, 2nd ed.; Oxford University Press: Oxford, UK, 1975.

[10] Vergnaud, J. *Controlled Drug Release of Oral Dosage Forms*; Ellis Horwood: New York, NY, USA, 1993.

[11] Lu, S.M.; Chen, S.R. Mathematical analysis of drug release from a coated particle. *J. Controlled Release* **1993**, *23*, 105–121.

[12] Hadjitheodorou, A.; Kalosakas, G. Analytical and numerical study of diffusion-controlled drug release from composite spherical matrices. *Mater. Sci. Eng. C* **2014**, *42*, 681–690.

[13] Kaoui, B.; Lauricella, M.; Pontrelli, G. Mechanistic modelling of drug release from multi-layer capsules. *Comput. Biol. Med.* **2018**, *93*, 149–157.

[14] Carr, E.J.; Pontrelli, G. Modelling mass diffusion for a multi-layer sphere immersed in a semi-infinite medium: application to drug delivery. *Math. Biosci.* **2018**, *303*, 1–9.

[15] Ford Versypt, A.N.; Braatz, R.D. Analysis of finite difference discretization schemes for diffusion in spheres with variable diffusivity. *Comput. Chem. Eng.* **2014**, *71*, 241–252.

[16] Wang, S.; Mahali, S.M.; McGuiness, A.; Lou, X. Mathematical models for estimating effective diffusion parameters of spherical drug delivery devices. *Theor. Chem. Acc.* **2010**, *125*, 659–669.

[17] Mohd-Mahali, S.; Wang, S.; Lou, X.; Pintowantoro, S. Numerical methods for estimating effective diffusion coefficients of three-dimensional drug delivery systems. *Numer. Algebra Control Optim.* **2012**, *2*, 377–393.

[18] Bielinski, C.; Kaoui, B. Numerical method to characterise capsule membrane permeability for controlled drug delivery. *Int. J. Numer. Methods Biomed. Eng.* **2021**, *38*, e3551.

[19] Barchiesi, E.; Wareing, T.; Desmond, L.; Phan, A.N.; Gentile, P.; Pontrelli, G. Characterization of the shells in Llayer-by-layer nanofunctionalized particles: a computational study. *Front. Bioeng. Biotechnol.* **2022**, *10*, 888944.

[20] Jiang, P.; Jacobs, K.M.; Ohr, M.P.; Swindle-Reilly, K.E. Chitosan-polycaprolactone core-shell microparticles for sustained delivery of bevacizumab. *Mol. Pharm.* **2020**, *17*, 2570–2584.

[21] Allyn, M.M.; Luo, R.H.; Hellwarth, E.B.; Swindle-Reilly, K.E. Considerations for polymers used in ocular drug delivery. *Front. Med.* **2022**, *8*, 787644.

[22] Dias, J.R.; Sousa, A.; Augusto, A.; Bártolo, P.J.; Granja, P.L. Electrospun polycaprolactone (PCL) degradation: an in vitro and in vivo study. *Polymers* **2022**, *14*, 3397.

[23] Bartnikowski, M.; Dargaville, T.R.; Ivanovski, S.; Hutmacher, D.W. Degradation mechanisms of polycaprolactone in the context of chemistry, geometry and environment. *Prog. Polym. Sci.* **2019**, *96*, 1–20.

[24] Lam, C.X.F.; Savalani, M.M.; Teoh, S.H.; Hutmacher, D.W. Dynamics of in vitro polymer degradation of polycaprolactone-based scaffolds: accelerated versus simulated physiological conditions. *Biomed. Mater.* **2008**, *3*, 034108.

[25] LeVeque, R.J. *Finite Difference Methods for Ordinary and Partial Differential Equations: Steady-State and Time-Dependent Problems*; SIAM: Philadelphia, PA, USA, 2007.

[26] Dorfman, K.D.; Daoutidis, P. *Numerical Methods with Chemical Engineering Applications*; Cambridge University Press: New York, NY, USA, 2017.

[27] Carslaw, H.S.; Jaeger, J.C. *Conduction of Heat in Solids*, 2nd ed.; Oxford University Press: New York, NY, USA, 1986.

[28] Ozisik, M.N. *Heat Conduction*, 2nd ed.; John Wiley & Sons: New York, NY, USA, 1993.

[29] Morton, K.W.; Mayers, D.F. *Numerical Solution of Partial Differential Equations*, 2nd ed.; Cambridge University Press: New York, NY, USA, 2005.

[30] Garcia, D. *Simpson's rule for numerical integration*, 2025 (accessed March 24, 2025). https://www.mathworks.com/matlabcentral/fileexchange/25754-simpson-s-rule-for-numerical-integration. MATLAB Central File Exchange.

[31] Van Kampen, E.; Vandervelden, C.; Fakhari, A.; Qian, J.; Berkland, C.; Gehrke, S.H. Design of hollow hyaluronic acid cylinders for sustained intravitreal protein delivery. *J. Pharm. Sci.* **2018**, *107*, 2354–2365.

[32] Sobol', I.M. Sensitivity estimates for nonlinear mathematical models. *Matematicheskoe Modelirovanie* **1990**, *2*, 112–118.

[33] Saltelli, A. Making best use of model valuations to compute sensitivity indices. *Comput. Phys. Commun.* **2002**, *145*, 280–297.

[34] Saltelli, A.; Ratto, M.; Andres, T.; Campolongo, F.; Cariboni, J.; Gatelli, D.; Saisana, M.; Tarantola, S. Variance-based methods. In *Global Sensitivity Analysis. The Primer*; John Wiley & Sons: Hoboken, NJ, USA, 2008; pp. 155–182. https://doi.org/10.1002/9780470725184.ch4.

[35] Morris, M.D. Factorial sampling plans for preliminary computational experiments. *Technometrics* **1991**, *33*, 161–174.

[36] Campolongo, F.; Cariboni, J.; Saltelli, A. An effective screening design for sensitivity analysis of large models. *Environ. Model. Softw.* **2007**, *22*, 1509–1518.

[37] Saltelli, A.; Ratto, M.; Andres, T.; Campolongo, F.; Cariboni, J.; Gatelli, D.; Saisana, M.; Tarantola, S. Elementary effects method. In *Global Sensitivity Analysis. The Primer*; John Wiley & Sons: Hoboken, NJ, USA, 2008; pp. 109–154. https://doi.org/10.1002/9780470725184.ch3.

[38] COMSOL. *Uncertainty Quantification Module Users Guide*, 2021 (accessed March 22, 2025). https://doc.comsol.com/6.0/doc/com.comsol.help.uq/UncertaintyQuantificationModuleUsersGuide.pdf.

[39] Beck, J.; Arnold, K., Matrix analysis for linear parameter estimation. In *Parameter Estimation in Engineering and Science*; John Wiley and Sons: Hoboken, NJ, USA, 1977; pp. 213–326.

[40] Chacin Ruiz, E.A.; Swindle-Reilly, K.E.; Ford Versypt, A.N. *LayeredSpheres_DDSdesign*, 2025. https://github.com/ashleefv/LayeredSpheres_DDSdesign.

[41] Avery, R.L.; Pearlman, J.; Pieramici, D.J.; Rabena, M.D.; Castellarin, A.A.; Nasir, M.A.; Giust, M.J.; Wendel, R.; Patel, A. Intravitreal bevacizumab (Avastin) in the treatment of proliferative diabetic retinopathy. *Ophthalmology* **2006**, *113*, 1695–1705.

[42] Carichino, L.; Guidoboni, G.; Kansara, V.; Ciulla, T.; Harris, A. Gene therapy bio-factory: mathematical modeling of the human eye pharmacokinetics. In *Applied Mathematical Analysis and Computations II*; Wanduku, D.; Zheng, S.; Zhou, H.; Chen, Z.; Sills, A.; Agyingi, E., Eds.; Springer Nature: Cham, Switzerland, 2024; pp. 47–64.

[43] Tosa, V.; Mercea, P., Solution of the the diffusion equation for multilayer packaging. In *Plastic Packaging: Interactions with Food and Pharmaceuticals*, 2nd ed.; Wiley-VCH: Weinheim, Germany, 2008; pp. 247–32.